

In 1998 the XVI International Conference on Raman Spectroscopy, held in Cape Town, South Africa highlighted the application of Raman spectroscopy in the study of Art and Archaeology, which at that time was a very novel research field. The papers presented at this conference dealt with fascinating study objects such as ivories, oriental manuscripts, gemmology, lichen from the antartic, Egyptian papyri, artefacts from the wreck of the *Pandora* and cave paintings in France, to mention but a few. Since then the applications in this field have grown dramatically, as illustrated in the figure below where the number of research papers published in this field from 1998 to 2007 is plotted against the publication year.

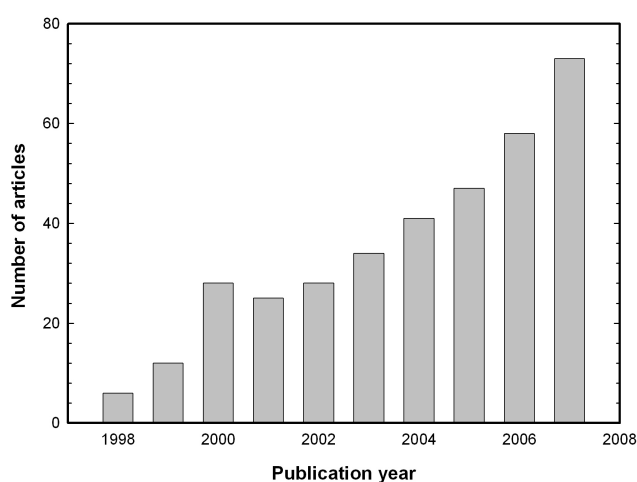


Figure 1: Growth of the number of research papers on Raman spectroscopy in art and archaeology (1998-2007), according to a survey on the Web of Science.

This thesis is based on the results of four studies in this research field, which was inspired by the conference; two on artefacts from the Mapungubwe collection and two on rock art. It is presented as four original articles published in the *Journal of Raman Spectroscopy* (Impact factor = 2.133) during the time span 2001-2008, together with a preceding chapter explaining the theoretical background used in the research.

Two of the studies were performed in collaboration with Ms Sian Tiley, the curator of the Mapungubwe Museum, which opened its doors in January 2000. In both studies imported artefacts excavated on Mapungubwe hill, namely celadon shards and glass trade beads, are investigated.

Imported glass beads, together with ceramics are the earliest and most abundant artefacts in the archaeological record, which clearly indicate international trade. Furthermore exotic

imports, when found in an archaeological context, have always provided a basic archaeological dating method if securely dated at their point of origin. In East Africa this is of cardinal importance since the only written records of the pre-Portuguese era consist of the Greek *Periplus Maris Erythraei* (2 AD), a few travel documents from Arab travellers and hearsay knowledge documented in Chinese sources. Two fragments of Chinese porcellaneous ware were excavated in 1934 during the first archaeological expedition to Mapungubwe and in 1991 another shard from the same vessel was found at the main entrance to Mapungubwe Hill. These shards and thousands of imported glass beads, mostly found in graves, connect Mapungubwe to the extensive maritime trade network, already established in the 1st century AD, which linked East Africa with the monsoon-based commercial systems of the Indian Ocean. Furthermore, the central position of Mapungubwe Hill, situated at the confluence of the Limpopo and Shashe rivers, also made it from the earliest times accessible via old camel caravan routes to Egypt and the Mediterranean trade. Likewise, trade along the African west coast was accessible via the interior, through Botswana and Angola, where Portuguese mariners had traded in beads imported from Europe 150 years before they rounded the Cape of Storms and also dominated the African east coast trade.

Therefore, research on the imported goods in the Mapungubwe Collection is of the utmost importance, as the discovery of the provenance of the artefacts would help to unravel the old trade routes through and around Africa. Indirectly it can also assist in refining the dating of the Mapungubwe archaeological site.

The other two studies followed after a field trip to the Mapungubwe Heritage site, where it became clear that Raman spectroscopy could also play a role in rock art research. San rock art sites are found throughout southern Africa; unfortunately this unique heritage is rapidly being lost through natural weathering processes as the paintings are mostly found in rocky shelters and underneath overhangs, which are exposed to the elements. This has led to various projects during which factors influencing natural weathering processes such as micro-climate, rock moisture and rock temperature have been studied. It is essential to know the chemical composition of the pigments and binders used by the San artists for the interpretation of rock weathering studies and it is also of primary importance for conservation purposes. Raman spectroscopy has been used successfully to analyse pigments and substrata in prehistoric rock art and it has been shown that it could also be useful in the study of San rock art deterioration.

In the concluding chapter the work is put in context and possible future research is discussed.

In this chapter the fundamentals of vibrational spectroscopy are described as it forms the theoretical basis of the analytical techniques used in all four studies. The focus of the discussion is micro-Raman spectroscopy as it was the main investigative technique. Infrared spectroscopy, inelastic neutron scattering and hyper Raman spectroscopy are briefly discussed as far as it is complementary to Raman spectroscopy. Resonance Raman spectroscopy is highlighted as it made it possible to detect nano-sized phases in rock art and glass. Raman spectroscopy of nanomaterials is illustrated through its application to the study of glasses and ceramic glazes; both materials with structural disorder at the nano-scale.

2.1 Fundamentals of vibrational spectroscopy

2.1.1 Vibrations in Crystalline Solids

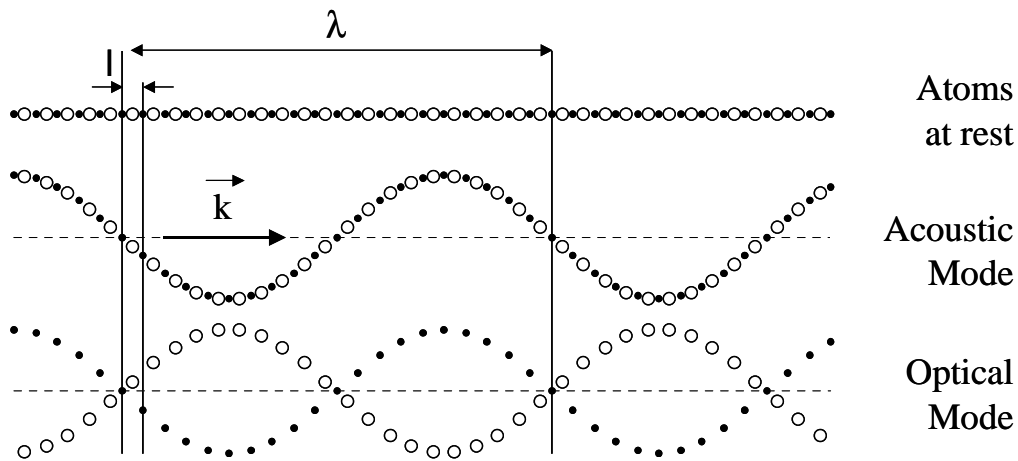
All collective vibrations that occur in crystals can be viewed as the superposition of plane waves that virtually propagate to infinity. These plane waves, known as normal modes of vibration, are commonly modelled by quasi-particles called *phonons*. A normal coordinate of the form $Q=Q_0\cos(2\pi\nu_{\text{vib}}t)$, a linear combination of bond lengths and bond angles, is associated with each normal mode (ν_{vib} = vibration frequency, t = time).¹ For structures containing isolated covalently bonded entities, the "molecular description" (see § 2.2.3) applies and in this case, depending on the dominant term in the normal coordinate, modes can be classified as stretching (**v**), bending (**δ**), torsional (**τ**), librational (**R'/T'** pseudo-rotations/translations) or lattice modes (the latter includes the relative displacement of the unit cells).

For a three-dimensional (3D) solid containing N unit cells with p atoms each, $(3pN-6)$ different phonons can propagate¹ and their wavevectors (\vec{k}) all lie in a volume of reciprocal space called the Brillouin Zone (BZ)². A phonon is characterised by its wave vector \vec{k} , with the length of the wave vector $|\vec{k}| = \frac{2\pi}{\lambda}$, where λ is the wavelength.² The direction of \vec{k} can be either parallel or perpendicular to the particle motions, giving rise to longitudinal phonons (L), which

¹ There are $3pN$ degrees of freedom but the 6 rotations and translations of the whole solid are not considered to be proper vibrations.

² The BZ describes the geometrical distribution of the wavevectors in reciprocal space in the same way the unit cell describes the geometry and periodicity of the crystalline arrangement in direct space.

are vibrations in the propagation direction and transverse phonons (T) with vibrations perpendicular to the direction of \vec{k} . Phonons can further be classified into acoustic (A) and optical (O) branches. The former represents modes with in-phase oscillations with the electron cloud and the latter modes with out of phase oscillations.³ The out-of-phase optical mode vibrations are associated with an electronic dipole moment, but the acoustic modes not. Consequently optical Raman modes are substantially stronger than acoustic ones. Fig. 1 is an illustration of the concept of phonons in crystals showing the transverse vibrations in a one-dimensional lattice where $p=2$.¹



³Figure 1: The transverse phonons ($|\vec{k}| = \frac{2\pi}{\lambda}$) in a 1D-solid with unit cell parameter l .

The energy of a phonon ($E = \nu \cdot h$, where ν is the frequency of the phonon and h is Planck's constant) is dependent on the length and direction of the wavevector and dispersion curves relating the frequency to the wavevector \vec{k} can be established with the use of neutron scattering experiments. The exact relationship between ν and \vec{k} depends on the masses of the atoms and elastic constant of the crystal.² If there is only one atom per unit cell, the phonon dispersion curves are represented only by acoustic branches. In the case of more than one atom per unit cell a greater number of vibrational modes are available and both acoustic and optical branches appear. Generally for a crystal with N atoms per primitive unit cell there will be 3 acoustic branches (1 longitudinal and 2 transverse) and $3N-3$ optical branches ($N-1$ longitudinal and $2N-2$ transverse).⁴ In Fig. 2 typical dispersion curves for a three-dimensional lattice, with partly ionic binding and cell length a are shown. Only the first Brillouin zone, $-\pi/a \leq \vec{k} \leq \pi/a$,

³ Figure 1 from reference 1.

needs to be considered as values from outside only reproduce motions of atoms already described for \vec{k} within these limits.⁴

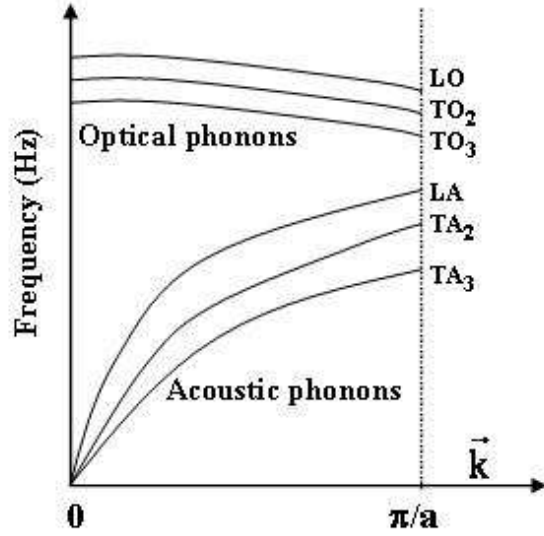


Figure 2: Typical phonon dispersion curves for the lattice vibrations, along a given crystallographic direction, of a three-dimensional anisotropic lattice with partial ionic binding.

Raman and infrared spectroscopy are the customary experimental methods to measure vibrational modes of materials. Neutron scattering is the only experimental method, which can be used to determine the dispersion curves, but is not commonly available.

2.1.2 The Raman Effect

The polarization of the dipoles excited in solids when a laser beam (amplitude E_0 ; frequency ν_{las}) interacts with phonons of frequency ν_{vib} depends on the polarisability tensor $\vec{\alpha}$:

$$\vec{P} = \vec{\alpha} \times \vec{E}_0 \cos(2\pi\nu_{\text{las}}t) \quad (1)$$

$\vec{\alpha}$ terms can be individually described as functions of the normal vibration coordinates Q using a Taylor approximation:⁵

$$\alpha_{ij} = \alpha_{ij}^0 + \left(\frac{\partial \alpha_{ij}}{\partial Q} \right)_{Q=Q_0} \times Q \quad (i, j = x, y \text{ or } z) \quad (2)$$

$$P_i = \sum_j \alpha_{ij} \times E_j = \sum_j \left[\alpha_{ij}^0 E_{0j} \cos(2\pi\nu_{\text{las}}t) + \frac{E_{0j} Q_0}{2} \left(\frac{\partial \alpha_{ij}}{\partial Q} \right)_{Q=Q_0} \times \left[\cos(2\pi(\nu_{\text{las}} - \nu_{\text{vib}})t) + \cos(2\pi(\nu_{\text{las}} + \nu_{\text{vib}})t) \right] + \dots \right] \quad (3)$$

With the scattered electric field proportional to \vec{P} , Eq. (3) predicts both quasi-elastic ($\nu \sim \nu_{\text{las}}$) and inelastic ($\nu = \nu_{\text{las}} \pm \nu_{\text{vib}}$) light scattering. The former is known as Rayleigh scattering and the latter, which occurs only if vibrations change polarisability ($\partial\alpha_{ij}/\partial Q \neq 0$), is Raman scattering.^{5,6} The Raman scattered light consists of a Stokes ($\nu = \nu_{\text{las}} - \nu_{\text{vib}}$), as well as an anti-Stokes branch ($\nu = \nu_{\text{las}} + \nu_{\text{vib}}$), which is illustrated in Fig. 3. Stokes scattering occurs when the initial vibrational state is the ground state, excitation takes place to a virtual state and decays to a real vibronic state with higher energy than the initial state, therefore the scattered photon has a lower energy than the incident photon. In anti-Stokes scattering the initial state is the excited state and the scattered photon has higher energy than the incident one. At room temperature the population of vibrational excited states is low according to the Boltzmann population of states, hence although the Stokes and anti-Stokes spectra contain the same frequency information, the Stokes spectrum is always more intense than the anti-Stokes spectrum and consequently generally used in Raman spectroscopy.

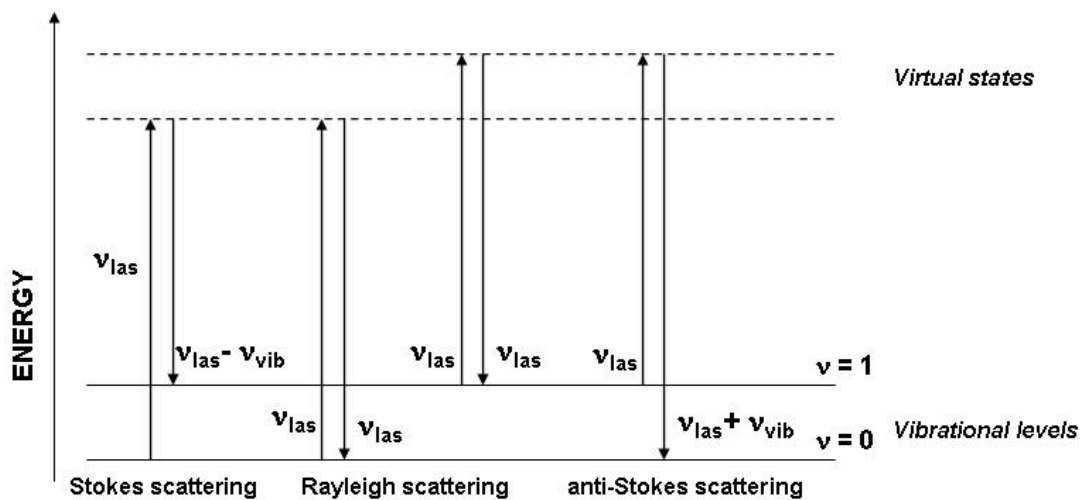


Figure 3: Illustration of linear Raman scattering processes

Raman spectroscopists normally refer to vibrational modes by their wavenumber $\bar{\nu} = \nu_{\text{vib}}/c$ (c the light speed, $\bar{\nu}$ in cm^{-1} unit) and the classical electromagnetic theory of radiations from an oscillating dipole demonstrates that Raman peaks have a Lorentzian shape.

$$I(\bar{\nu}) = I_0 \times \int_{(\text{BZ})} \frac{d^3\bar{k}}{[\bar{\nu} - \bar{\nu}(\bar{k})]^2 + \left(\frac{\Gamma_0}{2}\right)^2} \quad (4)$$

In Eq. (4), $\bar{\nu}(\bar{k})$ represents the dispersion branch to which the mode belongs and Γ_0 is the half-width for the ordered reference structure.

The scattering of one photon ($\bar{k} \sim \bar{0}$) by n phonons (wavevectors \bar{k}_i) is governed by the momentum conservation rule:

$$\sum_{i=1}^{i=n} \bar{k}_i = \bar{k}_{\text{scattered}} - \bar{k}_{\text{incident}} \approx \bar{0} \quad (5)$$

Therefore, only vibrations from the centre of the Brillouin zone, *i.e.* long wavelength phonons can be active in any one-phonon process (first order spectrum). However, not all of the phonons are active in Raman spectroscopy. According to Eq. (3), $\partial\alpha_{ij}/\partial Q$ terms must be different from zero and this condition is governed by the symmetry of the crystals.⁷

An interesting feature of Eq. (3) is to reveal the dual sensitivity of Raman spectroscopy to the electrical (α_{ij}) and mechanical (ν_{vib}) properties of the investigated materials.¹ Two kinds of parameters will therefore influence the spectra:

- (i) parameters acting on mechanical properties like atomic mass, bond strength or the system geometry (interatomic distances, atomic substitutions) will determine peaks positions (the eigenfrequencies of matter vibrations).
- (ii) parameters acting on the "charge transfer" (iono-covalency, band structure, electronic insertion) will determine intensity, on the basis of vibration-induced charge variations at atomic bond scale.¹

As polarisability changes for different kinds of bonds, Raman intensity is difficult to use for the quantitative determination of different phases. Covalent materials in general are good Raman scatterers, whereas ionic structures are more difficult to analyse with Raman spectroscopy. As for metals, their surface plasmons limit the penetration of light resulting in a very weak Raman signal.

The intensity of Raman scattering is given by the following equation:

$$I_R = I_0 K \nu_{\text{las}}^4 \left| e_0 \bar{\alpha} e_s \right|^2 d\Omega \quad (6)$$

where $\bar{\alpha}$ is the polarisability tensor, K a constant, e_0 and e_s the unit vectors defining the directions of the electric field of the exciting and scattered light respectively, $\bar{\nu}_0$ the energy of

the excitation laser and $d\Omega$ the collection solid angle.¹ From equation 6 it is clear that high energy lasers (blue or violet lines) and backscattering measurements (i.e. the use of a high magnification objective with large aperture) will enhance the intensity. The Raman cross-section could vary many orders of magnitude as a function of the nature of the bond and the exciting wavelength used.

2.1.3 Resonance Raman Spectroscopy

If the energy of the laser excitation (usually in the UV-nIR range) approximately matches the energy of an electric dipole allowed transition of the material under investigation (usually coloured material), a strong enhancement of some vibrational modes (near-resonance/resonance Raman scattering) can be expected. In other words, the virtual state energies of the Raman effect approaches that of the electronic excited states. Resonance can increase the intensity as much as a factor of 10^6 and concerns mainly the symmetric vibrational modes and their overtones and combinations.⁷

In chapter 6 this effect made it possible to identify nano sized quantities of two different carotenoids in San rock art paint as carotenoid pigments experience a strong resonance enhancement due to electron-phonon coupling of the π -electrons of the polyacetylenic backbone.⁷ In chapter 4 the presence of the Fe-S chromophore in black glass beads is also detected through a resonance effect.

2.1.4 Infrared spectroscopy

In infrared spectroscopy the nature of the light-matter interaction is not the same as in Raman spectroscopy and the fundamental differences between the two processes determine the selection rules, which control the Raman or infrared activity of a normal mode of vibration. Interaction of infrared radiation with a normal mode of vibration only occurs when the electric vector of the radiation field oscillates with the same frequency as instant dipoles caused by atomic vibrations. A normal vibration is therefore infrared active only if a change in the dipole moment of the vibration occurs and is a one-photon process, as only the photon absorbed is involved.⁷ Therefore infrared spectra offer additional information to that obtained from Raman spectra, where a change in polarisability is necessary for a normal mode to be active. Several authors have outlined group theoretical methods, by which the symmetries of the normal modes

of vibration of molecules and crystal lattices can be determined.⁸⁻¹¹ In general infrared spectroscopy probes polar modes (vibrations that modify existing dielectric dipole moments) and Raman spectroscopy non-polar modes.

2.1.5 Inelastic neutron scattering

Inelastic neutron scattering is the process by which neutrons collide with atomic nuclei and either gain or lose kinetic energy. In this it is conceptually very similar to Raman scattering, but there are significant differences. The major difference is that photons (electromagnetic radiation) interact primarily with the electrons of a sample, while neutrons interact with the nuclei. The strength of the interaction is very dependent on the particular nuclide involved, isotopes and spin states. Another difference is that the wavelength of the electromagnetic radiation used for Raman experiments in the visible or near UV region has wavelengths of hundreds of nanometers, while neutrons have wavelengths slightly less than 0.2 nm (room temperature).¹² This means that the size of the neutron is comparable to the spacing between atoms, therefore there are no "selection rules" as is the case for optical spectroscopy and all vibrational modes are active but modified by the atomic diffusion length. Except for localised modes of protonic species (H cross section is ~x80 that of other atoms), identification of modes is difficult and the spectrum consists of a vibrational density of states (VDOS).

2.1.6 The hyper Raman effect

Generally the induced electric dipole moment \vec{P} of a system is related to the electric field \vec{E} of the radiation by a power series (see also Eq. 3)

$$\vec{P} = \alpha \vec{E} + \frac{1}{2} \beta \vec{E} \vec{E} + \frac{1}{6} \gamma \vec{E} \vec{E} \vec{E} \dots \dots \quad (7)$$

where α is the polarizability, β the hyperpolarizability and γ the second hyperpolarizability. α , β and γ are tensors of rank 2, 3, 4, etc. respectively, \vec{E} is the electric field and $\vec{E} \vec{E}$ is the dyadic product of two electric fields etc.⁷ The non-linear terms in Eq. (7) are usually negligibly small, but when the electric field is sufficiently large as in the case of giant-pulse lasers (Q-switched), contributions from the second term in Eq. (7) are sufficiently intense to be detected and is called hyper Rayleigh ($2\nu_{\text{las}}$) and hyper Raman scattering ($2\nu_{\text{las}} \pm \nu_{\text{vib}}$).⁷ The hyper Raman effect is a three-photon process involving two virtual states of the scattering system (Fig. 4).⁷ Two laser

photons of frequency ($2\nu_{\text{las}}$) are simultaneously scattered to give photons with frequencies $2\nu_{\text{las}}$ (hyper Rayleigh) or $2\nu_{\text{las}} \pm \nu_{\text{vib}}$ (hyper Raman) when a vibration is excited or destroyed respectively. Thus, hyper Raman lines are found in the spectral neighbourhood of the second harmonic ($2\nu_{\text{las}}$) of the incident laser radiation. It should be mentioned that Rayleigh scattering always occurs, but hyper Rayleigh scattering only occurs if the scattering material does not have a centre of symmetry.⁷ Hyper-Raman spectroscopy is a very useful technique to study glass.

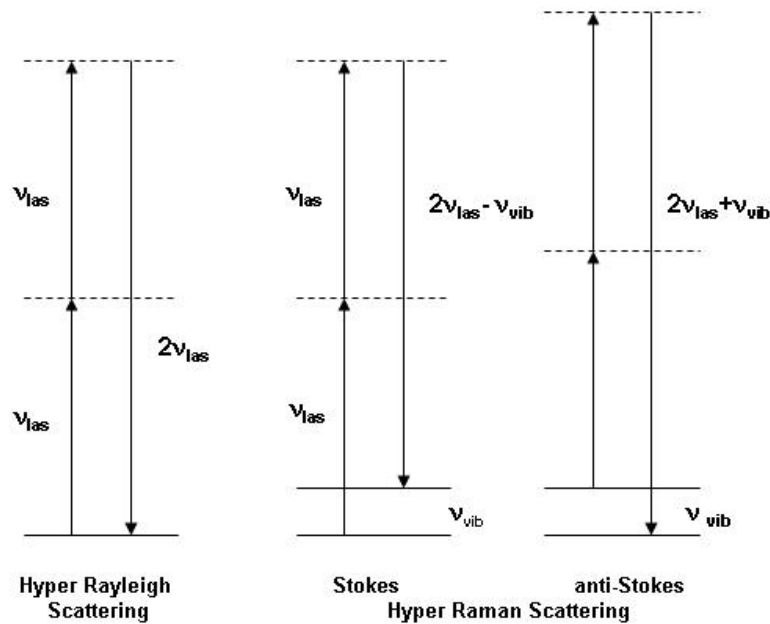


Figure 4: Schematic level diagram for hyper Rayleigh and hyper Raman scattering

2.2 Nanomaterials

Reducing the dimension of matter domains down to the nanometer scale confines the electronic and vibrational wavefunctions and vastly increases the ratio of surface area to volume, which results in unique properties of materials. It opens a wide range of potential applications in fields as different as optics, mechanics, electrical devices, magnetic devices, reactivity and biomedicine.¹

The challenge for nanotechnologists is to achieve perfect control of nanoscale-related properties. This obviously requires correlating the parameters of the synthesis process (self-assembly, microlithography, sol-gel, polymer curing, electrochemical deposition, laser ablation...) with the resulting nanostructure. Not every conventional characterization technique

is suitable for that purpose but the use of Raman spectroscopy has already been proven to be successful.¹

2.2.1 Raman spectroscopy of nanomaterials

The translational symmetry of crystalline materials is broken at grain boundaries, which results in the appearance of specific surface and interface vibrational contributions. These two factors are often neglected in Raman spectroscopy but become very significant in nano-crystals, where the concentration of grain boundaries is very high.¹

However, in many nanomaterials the Raman spectrum remains sufficiently similar to that of the corresponding single crystal to make direct identification of phases possible.¹³ Both crystallographers and Raman spectroscopists characterize disorder through peak broadening. Yet, while a loss of long distance translational periodicity is always associated with broadening for diffraction patterns, only lattice and librational (R', T') modes are sensitive to the same "long distance" disorder in Raman spectroscopy.¹³ The width of the other Raman modes is mainly sensitive to the "local" crystal field and if the "molecular" description of vibrations applies (see §2.9), then Raman bending modes are specifically sensitive to local geometric disorientation and Raman stretching modes to the neighbouring disorder (particularly atoms from other sublattices or electric defects resulting from substitutions/vacancies). Therefore the modifications of the vibrational signature is very small for stretching modes (bond lengths are very similar in crystals and amorphous materials), detectable for bending modes (sensitive to orientational disorder) and significant for librational and lattice modes (the lower energy motions) as only lattice modes reflect the long-range symmetry which determines the X-ray unit cell.¹

There are two ways of truly isolating the Raman signal coming from nano-particles. One is by having a nanoparticle to be the only one of its kind in the laser beam's path as is possible with Surface Enhanced Raman Spectroscopy (SERS), while the other involves a breaking of the $\lambda/2$ diffraction limit (Abbe criterion) of optical microscopes (nano-Raman). SERS is not always practical and the development of nano-Raman techniques is still in its infancy. However, although conventional Raman micro-spectrometers cannot provide laser spots smaller than $\sim 1\mu\text{m}^2$ the spectra stem from vibrations of chemical bonds.¹ This intrinsic "nanoprobing" makes Raman spectroscopy very sensitive to the short-range structure and qualifies it as a nano-analytical technique.¹³

2.2.2 Raman Microscopy

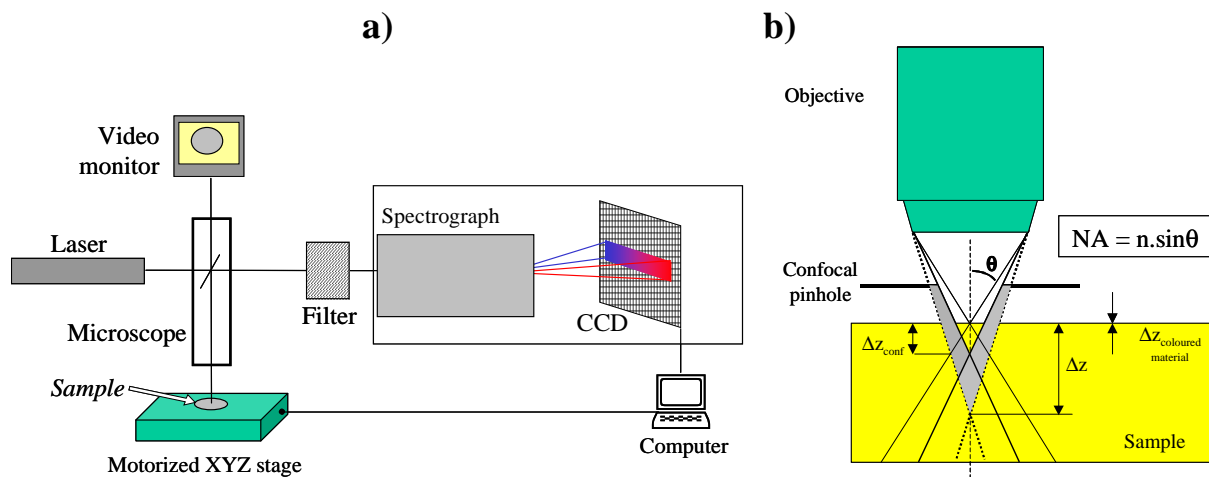
Up-to-date Raman equipment would include holographic gratings for improved excitation light rejection, a set of monochromators and a liquid nitrogen- or Peltier effect-cooled CCD detector (Fig 5a).⁶ The size of the sample analysed (laser spot) can be reduced to $\sim 1 \mu\text{m}$ diameter by using high-magnification microscope objectives. Owing to the diffraction of light, the intensity coming from a point observed through a microscope is distributed over an "Airy disk". The lateral resolution R , which is the smallest distance between two points to still appear distinctively on the microscope image, is half the width of the Airy disks. According to the Rayleigh criterion:

$$R = \frac{0.61 \times \lambda}{NA} \quad (8)$$

In Eq. (8), λ is wavelength of the light and NA represents the numerical aperture (Fig. 5b).

As for the axial resolution (Δz) of μRS , an estimate is given by the depth of field, which is defined as half the width of the axial intensity profile (modern instruments usually have a confocal hole which rejects the shadowed light and facilitates a more accurate in-depth analysis ($\Delta z_{\text{conf}} < \Delta z$)), which is approximated by the following equation:

$$\Delta z = \frac{\lambda}{n \sin^2 \theta} \Rightarrow \Delta z_{\text{through air (n=1)}} = \frac{\lambda}{(NA)^2} \quad (9)$$



⁴Figure 5: a) Illustration of a conventional micro-Raman spectrometer – b) Observation of a sample through a microscope (NA: Numerical Aperture; n is the refractive index of the medium separating the objective from the sample). A confocal hole rejects the shadowed light and facilitates a more accurate in-depth analysis ($\Delta z_{\text{conf}} < \Delta z$).

Under "standard" conditions ($n=1$, $\lambda=500\text{nm}$, $NA=0.5$), the typical lateral and in-depth resolutions of μRS are about $1 - 2 \mu\text{m}$. Even with the smallest visible wavelength ($\sim 400 \text{ nm}$) and

⁴ Figure 5 is from reference 1

the highest numerical apertures (oil immersion objectives with $n=1.515$; $NA\sim 1.4$), one should not expect a lateral resolution better than $R=0.2\ \mu\text{m}$ (the Abbe criterion states that the wave nature of light prevents the distinction of points closer than $\lambda/2$) and a field depth below $\Delta z=0.4\ \mu\text{m}$. Therefore a large amount of "nano-sources" contribute to the Raman signal.¹

2.2.3 Analysis of "isolated" vibrational units

Vibrational modes in crystals are extended plane waves. In contrast vibrational waves in disordered systems are never single plane waves and cannot be described in terms of a single \mathbf{k} -vector. Furthermore, for sufficiently large degrees of disorder, vibrational excitations may become spatially localised.¹⁴ In this case clusters of strong covalently bonded atoms are isolated from one another by weaker ionic bonds and thus become the relevant vibrational units (localized vibrations).¹⁵⁻¹⁷ All atoms from such a unit must exclusively belong to it for the normal coordinates of Eq. (2) & (3) to coincide with given bond lengths and bond angles. The spectra then consist of stretching and bending modes equivalent to the internal vibrations of polyhedral (mostly tetrahedral or octahedral) isolated molecules. The molecular scheme describes most organic polymers and also crystalline/amorphous inorganic polymers such as silicates, phosphates, carbonates, niobates, titanates and all compounds with polyatomic cations such as NH_4^+ , H_3O^+ or $\text{N}_2\text{H}_5^{2+}$.¹⁸⁻²⁰ A given vibration then always appears in the same region, its exact position giving information about the local environment of the corresponding bonds, both in the amorphous and crystalline state. Literature on silicate glass has to be read with caution as many authors simultaneously use several vibrational units. In a low polymerized silicate glass, i.e. in a depolymerised network where many Si-O bonds have been broken by silicon/sodium,

Table 1: Symmetry and main activity of a SiO_4 tetrahedron with T_d symmetry, C_{2v} site symmetry in a D_{6h} crystal structure.

Modes	Symbol	Symmetry T_d	Symmetry C_{2v} in D_{6h}	Main activity	Wavenumbers cm^{-1} SiO_4
Symmetric stretching	ν_1 or ν_s	A_1	$A_{1g}+E_{2g}+E_{1u}$	Raman	800-1000
Asymmetric stretching	ν_3 or ν_{as}	F_2	$E_{2g}+E_{1u}+E_{1g}+A_{2u}+A_{1g}$	IR	900-1200
Symmetric bending	ν_2 or δ_s	E	$A_{1g}+E_{2g}+E_{1u}$	Raman & IR	400-600
Asymmetric bending	ν_4 or δ_s	F_2	$E_{2g}+E_{1u}+E_{1g}+A_{2u}+A_{1g}$	IR	500-700
Rotational libration	R'			Raman & IR	300
Translational libration	T'			Raman & IR	100-200

potassium or lead substitution, the use of the SiO₄ tetrahedron as vibrational unit is a good choice. On the contrary in pure silica, where all oxygens belongs to 2 tetrahedra, the Si-O unit can be used.²¹⁻²³ Some authors prefer to use Si-O-Si units.²⁴ For instance the bending mode of SiO₄ tetrahedra can also be described as the scissoring mode of Si-O-Si units. An isolated SiO₄ tetrahedron has T_d symmetry and in an ordered structure with known site symmetry (eg. C_{2v}) and crystal structure (eg. D_{6h}) the main vibrational modes, Raman or infrared activity can be predicted by group theory (Table 1).

2.3 Application of Raman spectroscopy to ceramic glazes and glasses

2.3.1 The Raman spectrum of vitreous silica

In a classic paper Zachariesen proposed in 1932 that the interatomic distances (force constants) in glass and crystals must be similar as their mechanical properties are of comparable magnitude and that glass is also made up of a three-dimensional lattice, which is not symmetric or periodic (from the diffuse character of x-ray data).²⁵ Each atom in a glass network then has a unique position and the influence of the local environment on Si-O bonds is not dictated by the symmetry of the crystallographic site and space group as in a single crystal with a periodic structure. In fact as glass can be described as “liquid” from the physical point of view the influence of the surroundings on the Raman/IR spectrum can be compared to that of a solution on the spectra of solutes. This leads to a broadening of the vibrational modes as illustrated in Figure 6 (top: Raman, bottom: FTIR), where the spectrum of crystalline α -quartz is compared to that of α -quartz glass (the example is fulgerites form Witsand, Kalahari, South Africa). The broadness of the bands in the spectra of the glass is consistent with a statistical distribution of many different vibrations of varying strength. It is clear that the transformation from the crystalline to glassy phase is much more visible in the Raman spectrum than in the infrared. Due to the long-range interaction of electric dipoles, IR bands are much broader than their Raman counterparts, especially in a glassy material and only the small factor group splittings, observed in the crystalline spectrum (such as the characteristic 778/792 cm⁻¹ doublet of α -quartz), disappear in the amorphous one.

The broad bands in the spectra can readily be understood in terms of a continuous “random” network, but the two sharp peaks in the Raman spectrum commonly known as D₁ (495 cm⁻¹) and D₂ (606 cm⁻¹) modes are reminiscent of crystalline phases (Fig. 6, top). They have been assigned

by various authors to breathing modes of small 3 and 4 membered silicon cycles, which have decoupled from the network vibrations,²⁶⁻³⁰ but actually correspond to bending modes of nanocrystals, although protons also play a role.³¹ The other sharp peak in the spectrum of the glass at 458 cm⁻¹ belongs to nano sized crystallites of α -quartz (main peak at 462 cm⁻¹) imbedded in this natural glass, but its peak position has shifted to lower wavenumbers, indicating a lengthening of the Si-O bonds due to tensile stress experienced in the silica glass matrix. This arises from the

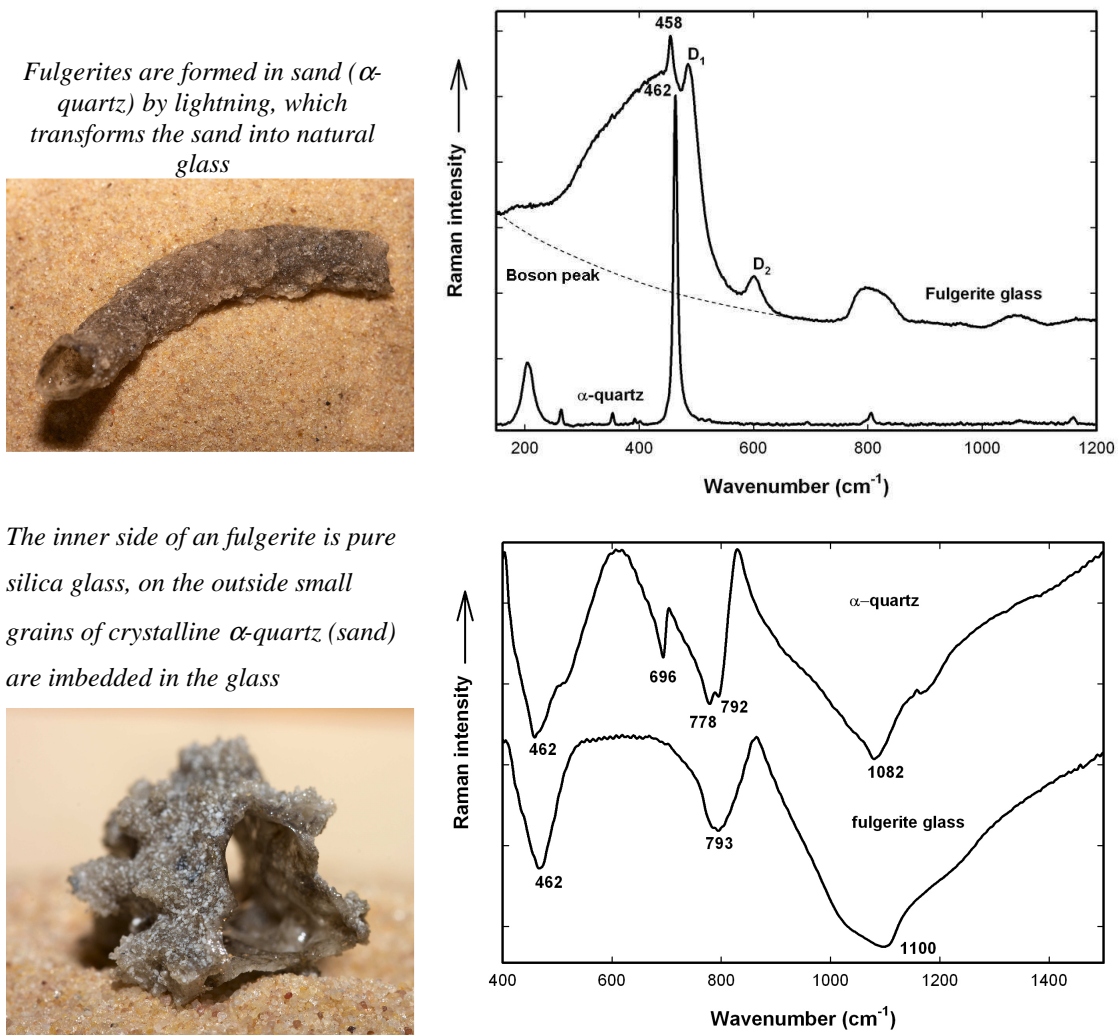


Figure 6: Comparison of the vibrational spectra of crystalline and glass quartz Raman (top) and FTIR (bottom)

thermal expansion mismatch between crystalline quartz, which for quartz is $\sim 60 \times 10^{-7} \text{ cm K}^{-1}$ and for amorphous glass $\sim 2 \times 10^{-7} \text{ cm K}^{-1}$. At high temperatures there is equilibrium between the two phases, but on cooling when the viscosity and fusing increase, the silica matrix experience very little thermal contraction, which is imposed on the quartz grain, hindering its normal contraction process. This causes the lengthening of the Si-O bonds in the quartz, which induces the

downshift. This phenomenon is also observed at the interface between a ceramic body and its glaze (see chapter3).

Also indicated on the figure is part of the Boson peak, which occurs between 0-100 cm^{-1} in all glasses (the rest of the peak is out of the detection limits of the instrument) and is so called as its intensity obeys a Bose-Einstein distribution. The origin of this peak has been highly debated by physicists³²⁻³⁶ but recent Hyper Raman measurements (see §2.1.6) confirm the assignment made by chemists, namely the Boson peak corresponds to the projection of lattice/external modes of the SiO_4 vibrational units similar to those in crystals.³⁷⁻³⁸ Various theoretical models have been proposed to remove the Boson peak, but essentially the results of these methods are very close to that obtained by using a four-point straight-line background subtraction.³⁹⁻⁴⁰

2.3.2 The Raman spectra of historic glass

The melting temperature of pure α -quartz glass is 1700°C which is not easily attainable for practical applications in the science, art and technology of glass, glazes and enamels. By adding fluxing agents (sodium, potassium, calcium, lead) the nanostructure of the three dimensional Si-O network is modified by replacing Si^{4+} covalently bonded atoms by non-covalent bonded atoms, hence decreasing the number of Si-O bridges and the connectivity of the network. Consequently, the firing temperature decreases and many other physical/chemical properties related to the density and network connectivity are modified accordingly.⁴¹

The transition from a highly connected tetrahedral structure (such as α -quartz glass, Fig.6, top) to weakly connected tetrahedral units, as caused by the addition of fluxing agents is reflected in the Raman spectrum by the appearance of a broad band in the region of Si-O stretching vibrations ($\sim 1000 \text{ cm}^{-1}$). This is analogous to the appearance of stretching vibrations in crystalline forms of silicates, where the network connectivity decrease in comparison with a fully connected α -quartz structure. Fig. 7 compares Raman spectra of the different classes of silicates such as nesosilicates (isolated SiO_4 tetrahedra eg. forsterite), sorosilicates (Si_2O_7 entities), cyclosilicates, innosilicates (chains), phyllosilicates (slabs) and tectosilicates (3D connectivity). It is clear that when going from a highly connected tecto-silicate to a neso-silicate without network connectivity, the ratio of stretching vibrations to bending vibrations increases.

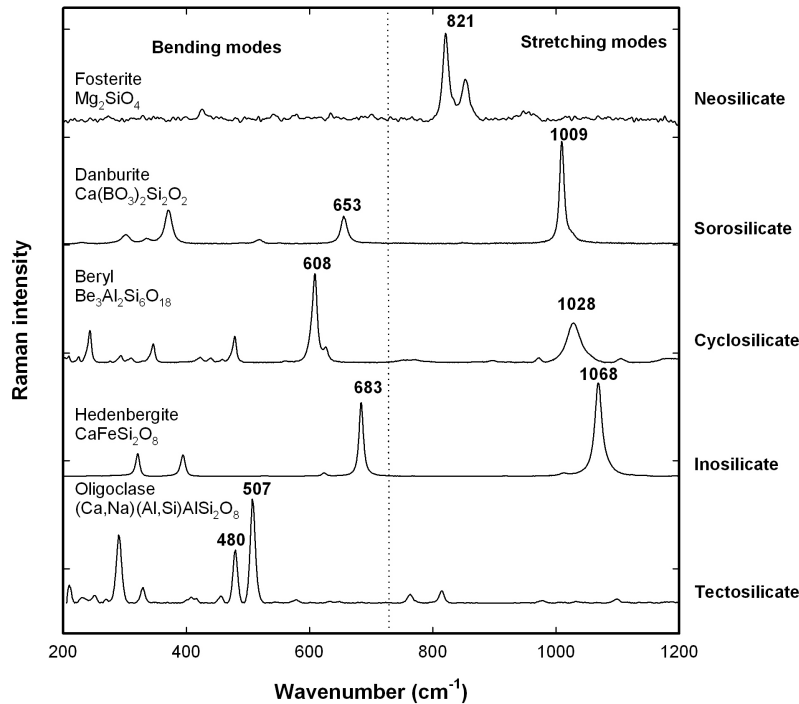


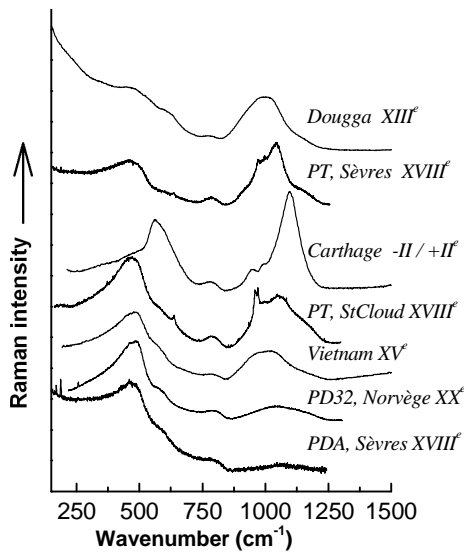
Figure 7: Raman spectra of various different crystalline silicates.

The Raman spectrum of a typical alumina/silica glass then consists of two broad bands around 500 and 1000 cm^{-1} . The band around 500 cm^{-1} , originates from the ν_2 bending vibration of SiO_4 tetrahedra and the one around 1000 cm^{-1} to coupled ν_1 and ν_3 Si-O stretching vibrations.^{39,42} As the amount of fluxing agents increases the Raman intensity of the bending modes decreases, while the stretching modes become more intense; reflecting a loss in the degree of polymerisation in the network. This is demonstrated in Fig. 8a where Raman spectra of glasses with different compositions, from a refractory silica-rich porcelain glaze (bottom) to a lead-rich glaze composition with a low melting point (top) are plotted showing the development of the band originating from the stretching modes.³⁹ Except for the broadness of the bands it mirrors the trend in Fig. 7 of the crystalline counterparts.

The relationship between the Raman index of polymerisation ($I_p = A_{500}/A_{1000}$ with A being the area under the Raman band), the glass composition and the processing temperature is well documented and has been used to classify glasses into various groups.^{39,42-44} In Fig. 8b it is shown how the Index of Polymerisation varies for different types of glass and in chapters 3&4 the use of this classification system is illustrated.

In many instances a comparison of the I_p of ancient glass/glaze samples with Fig. 8b (in reference 39) is sufficient to distinguish between two different glass technologies (see chapter 3), but to make a distinction between closely related technologies, it is necessary to analyse the

Raman spectrum further. In order to do this the broad bands of the glass spectrum has to be deconvoluted and the individual bands thus obtained assigned to different species or vibrational units according to a well-defined model.



⁵Figure 8a: Raman spectra of glasses having different compositions showing the development of the band originating from the stretching modes. (See details in ref 39)

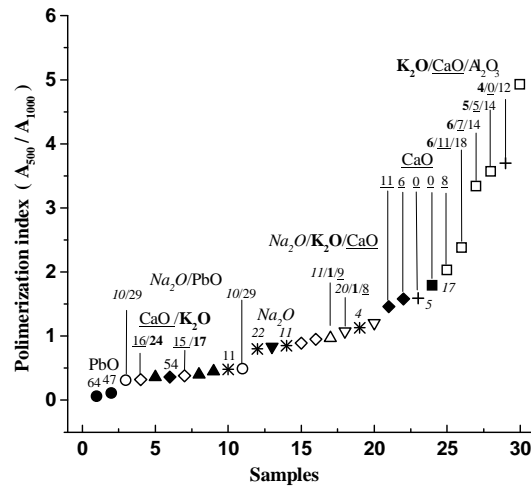


Figure 8b: Comparison of the Polymerisation index of different silicate glasses (See details in ref 39) Molar ratios of the fluxing oxides are indicated on the figure.

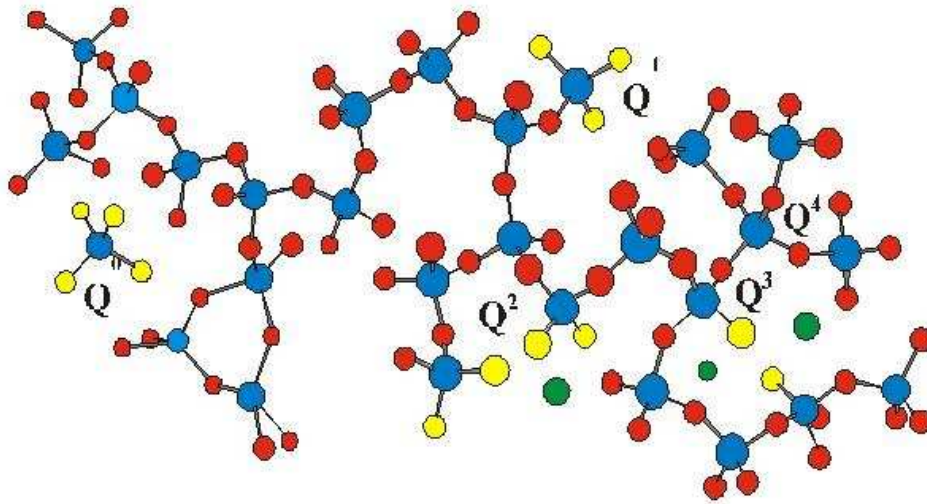
Historic glasses usually also have varying concentrations of aluminium (dependent on the composition of the sand used) as part of the network. On the basis of geometrical packing the ionic radius of Al is intermediate between the optimum radii for four-fold and six-fold coordination. Due to this factor and the amphoteric nature of aluminium, Al^{3+} can be either a network forming or network-modifying cation in aluminosilicate melts. As a tetrahedrally coordinated cation within a silicate network Al^{3+} is typically associated with a charge balancing cation such as an alkali or alkaline-earth cation.⁴⁵⁻⁴⁸ Because of the more ionic character of Al-O bond in comparison to the covalent Si-O bonds, its contribution to the Raman spectrum of aluminosilicate is close to nil.³⁹ Aluminium ions are thus not a glass forming species from the vibrational point of view and influence the silicate network in a similar way as other cations used as fluxing agents.

2.3.3 Defining a vibrational unit for glass: the Q_n model

A common nomenclature system known as the Q_n notation, where n is the number of bridging oxygens per tetrahedron, has been in use since the 70's.⁴⁸⁻⁵² A tetrahedron fully linked into the network via four bridging oxygens is designated as a Q_4 unit, while an isolated

⁵ Figure 8 a&b is from reference 39

tetrahedron with no bridging oxygens is designated as a Q_0 unit (Fig. 9). Based on the spectra of crystalline phases the positions of the various Q_n structures could be assigned to silica vibrations with zero (Q_0 , 800-850 cm^{-1} , compare fosterite), one (Q_1 , ~950 cm^{-1}), two (Q^2 , ~1020-1040 cm^{-1}), three (Q_3 , ~ 1100 cm^{-1}) and four (Q^4 , ~1150-1250 cm^{-1}) bridging oxygens per tetrahedral group.



⁶Figure 9: Sketch of a silicate framework. SiO_4 tetrahedron (Si^{4+} , large circle, O^{2-} ion small circle) can be isolated or connected by 1, 2, 3 or 4 oxygen atoms. Fluxing cations (Na^+ , K^+ , Ca^{2+} , ...) are represented by isolated circles.

The main advantage of the Q_n model is that it is applicable to all silicate compositions and is therefore a very realistic model. However the following assumptions are made:

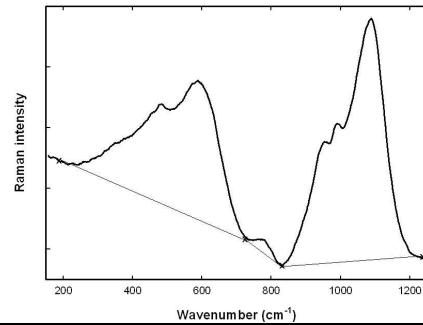
- i) only one symmetric mode is expected for a given Q_n tetrahedron, thus splitting due to site symmetry is neglected. Asymmetric modes are ignored (see Table 1),
- ii) it is assumed that the intensity of the above symmetric Q_n stretching mode does not vary with glass composition,
- iii) it is also assumed that the bandwidth of each component have similar values.

Note that the model implies that there are only 5 bands and that extra bands do not belong to the signature of the glassy silicate network. If additional components with narrow bandwidths are present, they could correspond to nanocrystals. Based on this a workable model for the analysis of any glass sample based on a silicate network consists four basic steps, illustrated in Table 2.

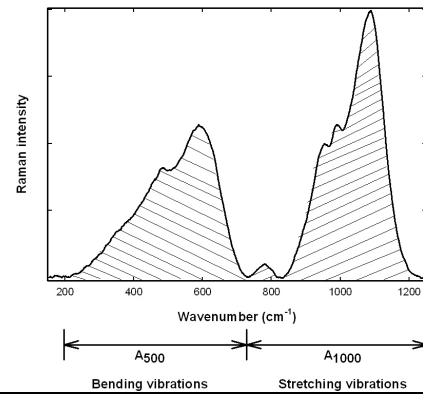
⁶ Figure 9 is from reference 1

Table 2: Procedures to determine the I_p and Q_n components from a glass spectrum

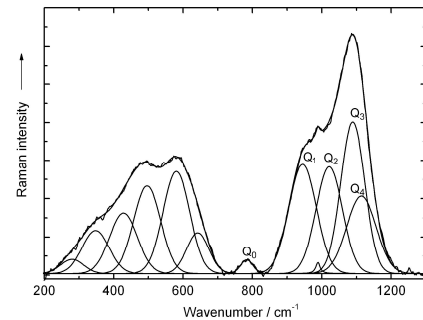
- a. A four-point baseline subtraction to remove contributions from the Boson peak and other fluorescence that may be present in very old samples



- b. Integration of the areas under the two peaks (LapSpec software of Dilor works well) and calculation of I_p and comparison with the existing database.



- c. Peak fitting of the stretching vibrations envelope by choosing 5 Gaussian components, with a restriction that the FWHM < 100. Sharp peaks are attributed to crystalline phases, chosen as Lorentzian, with a restriction of FWHM = 20. (The Origin Peakplot program was used in this study)



A combination of the I_p and various parameters determined through the deconvolution process, namely the wavenumber positions and areas Q_0 - Q_4 makes it possible to correlate the parameters in 2D diagrams and with chemometrics methods as illustrated in reference 39. This is a powerful tool that has been successful in distinguishing between production technologies of closely related ceramic glazes.³⁹

It is not only the modification of the silicon network (bond angles, force constants, etc.) that influences the Raman spectrum, but also the type of cation inserted within the matrix as fluxing agent. Both the size and oxidation state of the cation influence the bandwidth and position of the various peaks as illustrated by several authors.⁵²⁻⁵⁴ The merit of a Raman spectrum is that all of these effects are encapsulated in one single spectrum and by utilizing the method above makes it possible to analyse any unknown archeological glass object. In chapter 4 it was not possible to match the glass beads analysed exactly to a glass in the existing database,

but all the necessary parameters have been determined and published. Hopefully this will lead to identification later on, as the database is continuously expanding

2.3.4 Glass weathering

In many instances ancient glass samples have undergone changes due to weathering processes, of which an in-depth understanding is very important for conservation studies of museum glass, stained glass windows and archaeological glass artefacts. Alteration of the glass is attributed to a reaction between the glass surface and aqueous solutions (such as rain or groundwater) in a two-stage process. In the first stage there is an ion-exchange between protonic species from the liquid and an alkali ion that is removed from the surface of the glass and the formation of an alkaline wet film on the surface. This film becomes increasingly alkaline and above pH 9 the second stage occurs, with decomposition of the silicate network. In the Raman spectra this is evidenced by the main Si-O stretching vibration shifting to lower wavenumbers and a decrease in intensity of the Si-O bending vibration at $\sim 570\text{ cm}^{-1}$, the narrow component and 950 cm^{-1} and the Boson peak. In addition Raman modes involving hydrogen occur in ranges where there is no overlapping with the modes involving other elements due to the low atomic mass of hydrogen ($>1400\text{ cm}^{-1}$, typically). Also the bond potential between a proton and other atoms is very anharmonic and thus combinations and harmonics have significant intensities and due and can be observed between 4000 and 8000 cm^{-1} , some times up to $20\,000\text{ cm}^{-1}$. Thus OH^- and O-H^+ groups, H_2O , H_2 can be observed both by Raman and IR spectroscopy. This is very useful in following glass deterioration processes.⁵⁵⁻⁵⁸ In chapter 4 corrosion of glass beads could be identified through Raman spectra and water was detected in one bead with infrared spectroscopy, which differentiates it from other black beads with similar Raman spectra.

2.3.5 Pigments and (nano) crystalline inclusions

Glass colouring is obtained by doping the glass with $3d/4f$ ions or by the dispersion of coloured crystalline phases (pigments or metal nanoparticles) in the glass matrix. Colouring obtained by doping disperses ions (eg. Co) throughout the silicate matrix and in many instances no special Raman signal can be observed. Small crystallites is sometimes distinguishable under a microscope objective (especially in ancient glasses), which makes it possible to focus on the pigment directly and obtain a spectrum, which can be identified by comparing it with a spectra library of reference material. Since the first publication of a spectral library (56 inorganic

pigments used before 1850) various other libraries have been compiled and are readily available through the internet. A detailed account of useful databases can be found in reference 59. Other crystalline second phases, such as opacifiers (eg. SnO_2), crystallites formed during the production process (eg. wollastonite) or phases inherent in the starting material (eg. TiO_2 -see chapter 3) can also be identified and may help in tracing the provenance of an artefact. In the rock art studies the identification of crystalline phases is richly illustrated.

References:

1. Gouadec G and Colomban Ph, *Prog Cryst Growth Ch.* 2007; **53**: 1-56.
2. Nissum M, Shabanova E and Nielson OF, *J. Chem. Ed.* 2000; **77**: 633.
3. Brink J, Honours Optics, Course Notes, University of Pretoria; 1998.
4. Cheetham AK and Day P, *Solid State Chemistry: Techniques*
5. D.A. Long, *Raman Spectroscopy*, McGraw-Hill International Book Company, London York 1977.
6. I.R. Lewis and H.G.M. Edwards (Eds.) *Handbook of Raman Spectroscopy - From the Research Laboratory to the Process Line*, Marcel Dekker Inc., NY, USA (2001).
7. Schrader B, *Infrared and Raman Spectroscopy*, John Wiley & Sons Ltd, London, 1995.
8. Ferraro JR and Zioemek JS, *Introductory Group Theory and its Applications to Molecular Structure*, Plenum Press, New York, 1969.
9. Adams DM and Newton DC, *Tables for Factor Group and Point group Analysis*, Beckman-RIIC Ltd, Croyden, England, 1970.
10. Rousseau DL, Bauman RP and Porto SPS, *J. Raman Spectrosc.* 1981; **10**: 253.
11. Fateley WG, Dollish FR, McDewitt NT and Bentley FF, *Infrared and Raman Selection Rules for Molecular and Lattice Vibrations, The Correlation Method*, John Wiley & Sons Ltd. London, 1995.
12. Dorner B, *Coherent Inelastic Neutron Scattering in Lattice Dynamics*, Springer-Verlag, 1982, Berlin.
13. Gouadec G and Colomban Ph, *J. Raman Spectrosc.* 2007; **38**: 598.
14. Taraskin SN and Elliott SR, *Physica B*, 2002; **316-317**: 81.
15. Condrate RA, *J. Non-Crystal. Solids* 1986; **84**: 26.
16. Colomban Ph, Glasses, Glazes and Ceramics – Recognition of the Ancient Technology from the Raman Spectra, in *RAMAN SPECTROSCOPY IN ARCHAEOLOGY AND ART HISTORY*, Ch13 pp 192-206, H.J. Edwards and J.M. Chalmers (Eds), 2004, Royal Society of Chemistry, UK
17. Faurel X, Vanderperre M, Colomban Ph, *J. Raman Spectrosc.* 2003; **34**: 290.
18. Griffith WP, *J. Chem. Soc. (A)* 1970; 286.
19. Griffith WP, *Nature* 1969; **224**: 264.
20. Griffith WP, *J. Chem. Soc. (A)* 1969: 1372.
21. Galeener FL, Lucovsky G, *Phys. Rev. Lett.* 1976; **37**: 1474.
22. Galeener FL, *J. Non- Crystal. Solids* 1990; 123: 182.
23. Galeener FL, Sen PN, *Phys. Rev. B* 1978; **17**: 1928.

24. Zachariassen WH, *J. Am. Chem. Soc.* 1932; **54**: 3841.
25. Handke M, Mozgawa W, *Vibr. Spectrosc.* 1993; **5**: 75.
26. Elliott R, *J. Non-Crystal. Solids* 1995; **182**: 1.
27. Galeener FL, *J. Non-Crystal. Solids* 1982; **49**: 53.
28. Galeener FL, Barrio RA, Martinez E and Elliot RJ, *Phys. Rev. Lett.* 1984; **53**: 2429.
29. Galeener FL and Thorpe MF, *Phys. Rev. B*, 1983; **28** (10): 5802.
30. Sitarz M, Mozgawa W and Handke M, *J. Mol. Struct.* 1999, **511-512**, 281-285.
31. Humbert B, Burneau A, Gallas JP, Lavalley JC, *J. Non-Crystal. Solids* 1992; **143**: 75.
32. Hassan AK, Börjesson L, Torell LM, *J. Non-Crystal. Solids* 1994; **172-174**: 154.
33. McInstosh C, Toulouse J and Tick P, *J. Non-Crystal. Solids* 1997; **222**: 335.
34. Taraskin SN, Loh YL, Natarajan G and Elliott SR, *Phys. Rev. B* 86 2001; **7**: 1255.
35. Inamura Y, Arai M, Yamamuro O, Inaba, Kitamura N, Otomo T, Matsuo T, Bennington SM, Hannon AC, *Physica B* 1999; **263-264**: 299.
36. Schroeder J, Wu W, Apkarian JL, Lee M, Hwa L-G, Moynihan CT, *J. Non-Crystal. Solids* 2004; **349**: 88.
37. Hehlen B, Courtens E, Yamanaka A and Inoue K, *J. Non-Crystal. Solids* 2002; **307-301**: 87.
38. Hehlen B, Courtens E, Vacher R, Yamanaka A, Kataoka M and Inoue K, *Phys. Rev. Lett.* 2000; **84**(23): 5355.
39. Ph. Colomban, A. Tournié, L. Bellot-Gurlet, *J. Raman Spectrosc.* 2006; **37**: 841.
40. B.O. Mysen, L.W. Finger, D. Virgo & F.A. Seifert, Curve-fitting of Raman spectra of silicate glasses, *Am. Mineral.* **67** 696-717 (1982).
41. Shelby JE, *Introduction to Glass Science and Technology*, 2nd Edition, The Royal Society of Chemistry, Cambridge, 2005.
42. Ph. Colomban, *J. Non-Crystalline Solids* 323 [1-3] (2003) 180-187.
43. Colomban, Ph, *Appl. Phys. A*, 2004; **79**: 167.
44. Colomban Ph and Paulsen O, *J. Am. Cer. Soc.* 2005; **88** (2): 390.
45. Rokita M, Handke, W and Mozgawa W, *J. Mol. Struct.* 1999; **511-512**: 277.
46. Mozgawa W, Handke Mand Jastrzębski, *J. Mol. Struct.* 2004; **704**: 247.
47. Tarte P, Rulmont A, Liégeois-Duyckaerts M, Cahay R and Winand JM, *Solid State Ionics*, 1990; **42**: 177.
48. Sharma, SK, Simons B and Yoder Jr. HS, *Am. Mineral.* 1983; **68**: 1113.
49. Mysen BO, Virgo D & Scarfe CM, *Am. Mineral.* 1980; **65**: 690.
50. Seifert F, Mysen BO & Virgo D, *Am. Mineral.* 1982; **67**: 696.

51. MacMillan PF, *Am. Mineral.* 1984; **69**: 622.
52. Brawer S, *Phys. Rev. B*, 1975; **11**: 3173.
53. Sitarz M, Handke M, Mozgawa W, Galuskin E and Galuskina I, *J. Mol. Struct.* 2000; **555**: 357.
54. Brawer S and White WB, *J. Non-Cryst. Solids*, 1977; **23**: 261.
55. Colombaro Ph, Etcheverry M, Asquier M, Bounichou M and Tournié A, *J. Raman Spectrosc.* 2006; **37**: 841.
56. Tournié A, Ricciardi P and Colombaro Ph, *Solid State Ionics*, 2008 submitted.
57. Robinet L, Coupry C, Eremin Kand Hall C, *J. Raman Spectrosc.* 2006; **37**: 789.
58. Robinet L, Coupry C, Eremin Kand Hall C, *J. Raman Spectrosc.* 2006; **37**: 1278.
59. Vandenberghe P, Edwards HGM and Moens L, *Chem. Rev.* 2007; **107** (3): 675.